Fifth International Conference on CFD in the Process Industries
CSIRO, Melbourne, Australia
13-15 December 2006

THE VORTEX TRAJECTORIES INVOKED BY AN ARRESTING CYLINDER

Gregory J SHEARD[1], Thomas LEWEKE[2] and Kerry HOURIGAN[1]

[1] Fluids Laboratory for Aeronautical and Industrial Research (FLAIR), Department of Mechanical Engineering, Monash University, VIC 3800, AUSTRALIA

[2] Institut de Recherche sur les Phénomènes Hors Équilibre (IRPHÉ), UMR 6594 CNRS / Universités Aix-Marseille I & II, 49, rue Frédéric Joliot-Curie, B.P. 146, F-13384 Marseille Cedex 13, FRANCE

ABSTRACT

The vortex dynamics of a translating circular cylinder which is rapidly arrested is investigated. Simulated particle tracking is employed to identify the trajectory of both the wake vortex pair, and the secondary vortices which are induced as the wake convects over the cylinder. In a similar fashion to the flow past an arresting sphere, each wake vortex induces a counter-rotating vortex, which subsequently self-propel over a range of sometimes surprising trajectories, as the Reynolds number and cylinder translation distance are varied. The results of these simulations have an application in small-scale mixing technologies. At low Reynolds numbers and short translation distances, the wake vortices propel past the cylinder, continuing in the direction of the original cylinder motion. At higher Reynolds numbers, the vortices deviate outwards in circular arcs of increasing curvature, to the point where the vortex pairs collide behind the cylinder. At longer translation distances, Hopf instability destroys the reflective symmetry about the wake centreline.

NOMENCLATURE

L/D	distance of cylinder travel / cylinder diameter
U	cylinder velocity prior to arrest
Re	Reynolds number
ν	kinematic viscosity
t	non-dimensional time
t_0	initial time
t_{arrest}	time at arrest

INTRODUCTION

The acceleration from, and deceleration to, zero velocity for a body in a fluid is applicable to widespread applications spanning vehicular aerodynamics, mixing, propulsion, ballistics and multi-phase fluid mechanics. While the case of an impulsively started body has been studied extensively (Braza, Chassaing & Ha Minh, 1986; Koumoutsakos & Leonard, 1995) in relation to the motion of circular cylinders in a fluid, the case of an arresting body has received limited attention (exceptions include Tatsuno & Taneda, 1971; Wang & Dalton, 1991). In these studies, the flows obtained were consistent: while the cylinder was in motion a recirculating wake comprising an attached counter-rotating vortex pair was observed. Subsequent to arrest of the cylinder motion, the momentum in the surrounding fluid carried the wake back over the cylinder, and this process induced secondary vortices which paired with each wake vortex in the vicinity of the widest point around the cylinder. The trajectories of these vortices over longer times have not been established to date. The studies did detect a variety of flow patterns depending on factors such as the speed and length of translation of the cylinder. This study intends to investigate systematically the flow regimes that develop around arresting cylinders for a wide range of Reynolds numbers and translation distances. The study will also track the flows for a significant amount of time after the arrest, to expand on trajectory traces presented in previous studies.

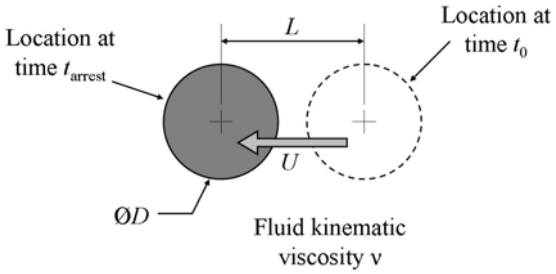

Figure 1: Schematic diagram of the arresting cylinder system, showing initial and final cylinder locations.

DEFINING THE ARRESTING CYLINDER PROBLEM

The arresting cylinder system consists of a two-dimensional circular cylinder that is initially at rest in a quiescent fluid. At time t_0, the cylinder impulsively initiates a translation (the *translating phase*), before returning to rest (the *arresting phase*). During the translating phase the cylinder travels a non-dimensional distance L/D, where L is the distance travelled, and D is the cylinder diameter. In the arresting phase, the cylinder is decelerated linearly from a velocity U to zero over $0.1D/U$ time units. Based on the velocity of translation, a Reynolds number may be defined

$$Re = \frac{UD}{\nu}, \tag{1}$$

where ν is the kinematic viscosity of the surrounding fluid.

Subsequent to the arresting phase is the stationary phase, during which residual motion in the fluid dissipates.

In figure 1 a schematic diagram demonstrates the relevant dimensions and parameters of the system under investigation.

NUMERICAL METHODOLOGY

This investigation was conducted using a spectral-element software package developed within the Department of Mechanical Engineering, Monash University, named *Viper*. Spectral element simulations are notable for their ability to compute on sparse meshes thanks to the high spatial order within each element through incorporation of high-order polynomials representing the flow variables, and efficient quadrature techniques. These features enable approximately spectral spatial convergence to be achieved (Karniadakis & Sherwin, 2005). Spectral element methods have been spectacular in their suitability for solving laminar incompressible bluff-body flow problems (see, for example: Thompson, Hourigan & Sheridan, 1996; Sheard, Thompson & Hourigan, 2003), as the multi-element feature permits flows in complex geometries to be modelled, and the high-order polynomials representing the flow variables match closely with the smooth variation in the physical flows.

The Spectral-Element Code

This code permitted two-dimensional calculations of time-dependent incompressible fluid flows on a mesh comprising curvilinear quadrilateral spectral elements. In a fashion similar to Thompson, Hourigan & Sheridan (1996), a nodal spectral-element formulation is employed, with velocity and pressure fields being evaluated at points corresponding to the Gauss-Legendre-Lobatto quadrature points. This allows for efficient computation of the solution as the equations of motion are solved in a weak form following application of the method of weighted residuals, with the test and trial functions occupying the same polynomial space. For time integration, a third-order accurate time splitting scheme based on a backwards-multistep integration method is employed (Karniadakis, Israeli & Orszag, 1991).

Simulated Particle Tracking

For visualization purposes, a numerical analogue to laser-induced fluorescent dye visualization (e.g., see Williamson, 1988) was implemented in the form of a nearly fourth-order time-accurate simulated particle tracking technique. In this technique, simulated particles are injected regularly into the flow in the vicinity of the cylinder, thus mimicking the entrainment of a dye from the body into the moving fluid. The new locations of these particles are calculated at regular time intervals as the simulation of the underlying flow progresses. Particle tracking is performed by updating particle positions within elements using a 4th-order Runge-Kutta time integration scheme in parametric space, while a linear series of substeps is employed to step to and across element interfaces (Coppola, Sherwin & Peiró, 2001).
Visualization of the particle tracking data was performed by calculating particle concentrations in the vicinity of each interpolation point used for plotting. Particle concentration was calculated based on a Gaussian distribution about each interpolation point, with a variance chosen based on the local mesh refinement. The goal is to simulate the softness in dye streaks observed in experimental visualization due to both the diffusion of the dye in the water, and the dazzling luminescence of high-concentration regions of dye. Tests verified that this technique provided images closely matching photographs of laser-fluoresced dyes in water, facilitating the direct comparison between experimentally obtained flows, and the computational equivalent computed in this study.

PARAMETER SPACE UNDER INVESTIGATION

Limited experiments have shown that there is a marked variation in flow states possible when either the Reynolds number or the translating distance (L/D) is varied. It is well known that above Re = 48 (Provansal, Mathis & Boyer, 1987) the wake of a circular cylinder transitions from a steady two-dimensional wake comprising a counter-rotating vortex pair attached to the rear of the cylinder, to a periodic wake comprising a street of shed vortices. This transition point affects the possible flow states of the arresting cylinder problem, as for long translation distances (e.g., L/D > 50-80) above this transition Reynolds number, the initially symmetric vortex pair will develop asymmetry due to this Hopf instability. A further limitation on the valid parameter space is the transition point for three-dimensionality. For a fully-developed wake behind a circular cylinder, this transition occurs at approximately $Re = 188.5$ (Barkley & Henderson, 1996), but in this system the three-dimensional transition is not known, as for most L/D ratios the wake and surrounding flow is highly transient and immature in its development. Therefore a range of Reynolds numbers will be investigated that includes values higher than the eventual transition point $Re \approx 2 \times 10^2$.
The Reynolds number range to be studied in this investigation is

$$50 < Re < 1000,$$

and the translation distance ratio range to be studied is

$$1 < L/D < 60.$$

WAKES AT THE POINT OF ARREST

For each computation, the injection points were fixed at locations $0.05D$ from the cylinder surface at the widest point around the cylinder normal to the direction of motion. Because of this, the speed with which particles entrained into the wake varied with Reynolds number. Due to the varying thickness of the boundary layer around the cylinder, an increase in Reynolds number caused an increase in the velocity at the injection point, which in turn increased the velocity of the entraining particles, and hence the distance the particles travelled over a given amount of time.
In figure 2, a series of images shows the entrainment of particles into the wake of a cylinder at the point of arrest for $L/D = 3$ for a range of Reynolds numbers. Notice that with an increase in Reynolds number, a longer thread of particles is observed to spiral into the core of the developing recirculating wake vortices. It is interesting to also note that despite the majority of these images being captured at Reynolds numbers beyond the nominal transition point for unsteady flow, each of these images retains symmetry about the wake centreline, suggesting that the Hopf transition has had insufficient time to develop.

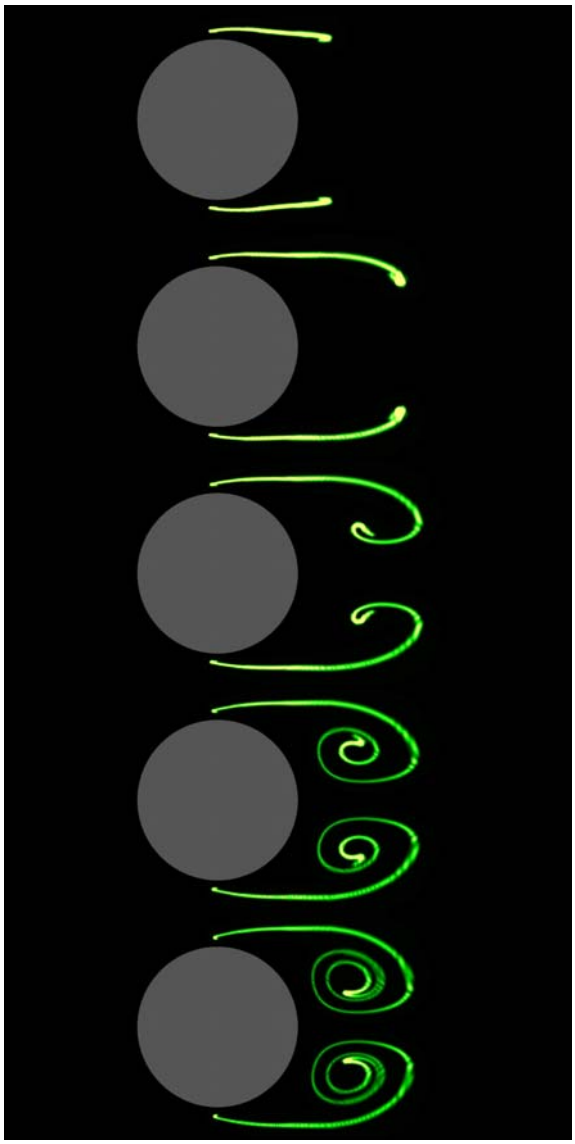

Figure 2: Wakes at the point of arrest with $L/D = 3$ at Reynolds numbers (top to bottom) $Re = 50$, 100, 200, 500 and 1000. Prior to arrest, the cylinder was moving from left to right.

Keeping the Reynolds number constant and varying the translation distance produces a range of wakes which differ significantly at the point of arrest. Here an increase in L/D increases the duration of translation, and hence the wakes are similar to instantaneous snapshots of the developing wake behind a circular cylinder. A Reynolds number of $Re = 100$ was chosen to reveal any deviation from symmetry due to the development of the Hopf instability in the cylinder wake. Figure 3 shows a series of images of the wakes at the point of arrest with constant Reynolds number and varying translation distance. For the shorter translation distances ($L/D \leq 10$) the wake remains symmetrical about the wake centreline, but for $L/D = 60$, the wake exhibits the early stages of the development of a Kármán vortex street, with broken wake centreline symmetry.

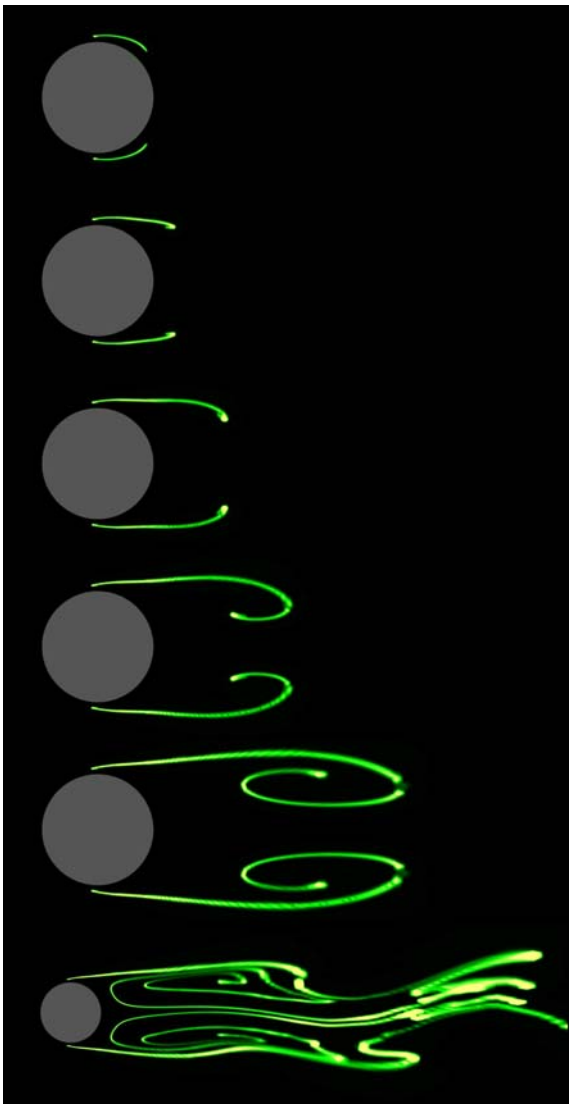

Figure 3: Wakes at the point of arrest with $Re = 100$ and translation distance (top to bottom) of $L/D = 1$, 2, 3, 5, 10 and 60. Prior to arrest, the cylinder was moving from left to right.

VORTEX DYNAMICS IN THE STATIONARY PHASE

Following the arrest of the cylinder motion, the developing wake vortices are carried towards and around the circular cylinder by the momentum in the surrounding fluid. Past studies (Leweke, Thompson & Hourigan, 2004) have shown that for an arresting sphere, this backflow of the wake vortices causes induced counter-rotating vortices to develop at the surface of the body, pairing with each passing wake vortex. The present computations have revealed a rich variety of vortex dynamics in the surrounding fluid for arresting circular cylinders with variation in both Reynolds number and translation distance.

At lower Reynolds numbers, the strong viscous diffusion causes a very rapid decay of the residual motion towards a steady state. The images in figure 4 demonstrate the effect of Reynolds number changes on the flow patterns at several times following arrest for cylinders with translation distance $L/D = 3$.

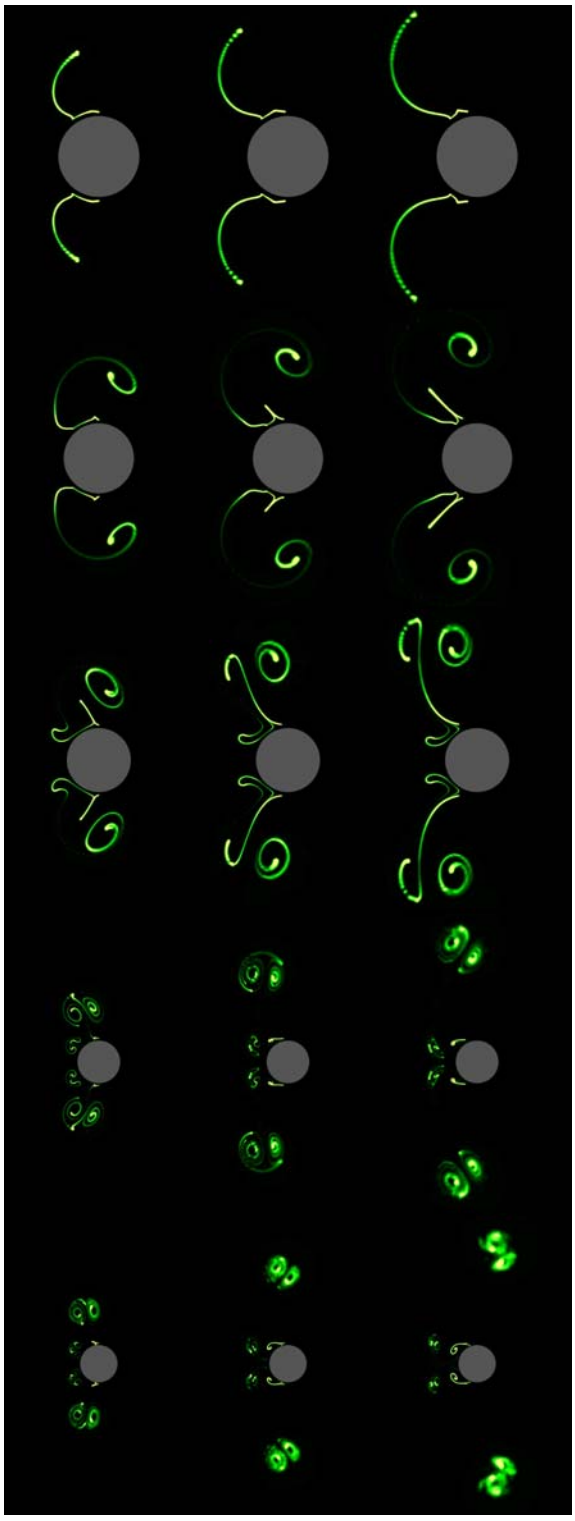

Figure 4: Flows at times t-t_{arrest} = 3, 6 and 9 after arrest (left, centre and right images, respectively), with constant L/D = 3, at Reynolds numbers Re = 50, 100, 200, 500, 1000 (top to bottom, respectively). For each sequence a different scale is used to magnify the relevant flow features. Prior to arrest, the cylinder was moving from left to right.

Several striking observations can be made about the vortex dynamics illustrated by the flows in figure 4. Firstly, notice that with an increase in Reynolds number, the simulated dye is drawn greater distances from the cylinder. It is apparent, especially from the simulations at Reynolds numbers Re = 200 and above, that the backwash of the wake vortices over the cylinder induces a secondary counter-rotating vortex of a similar but not equal magnitude. These primary and secondary vortices pair up and self-propel away from the cylinder. Due to the circulation discrepancy between the primary and secondary vortices in each pair, the trajectory of the pair is curved, and in each case this curvature trends away from the original direction of cylinder motion. The speed of this vortex-pair convection increased with Reynolds number, increasing the distance travelled. It is apparent at higher Reynolds numbers that at the formation of the secondary vortices leads to the formation of smaller vortex features near the upstream surface of the cylinder. Figure 5 provides a detail view of these features at Re = 500 over the same time intervals as used in figure 4.

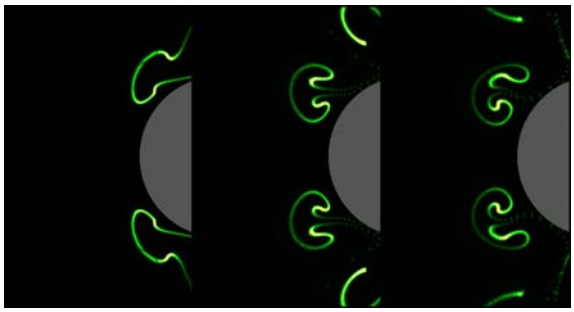

Figure 5: Detail view of the upstream surface of the cylinder at times t-t_{arrest} = 1, 2 and 2 after arrest (left, centre and right images, respectively), with constant L/D = 3, at Reynolds numbers Re = 500. Prior to arrest, the cylinder was moving from left to right.

The small vortex structures shown in figure 5 are counter-rotating pair vortices, which appear to develop as a result of the injection of narrow jets of fluid from over the downstream surfaces of the cylinder, likely a by-product of the formation of the strong secondary vortices pairing with the wake vortices.

VORTEX TRAJECTORIES IN THE STATIONARY PHASE

The plot in figure 6 shows the loci of the cores of both the primary wake vortex and the secondary induced vortex over times $0 < t\text{-}t_{arrest} < 24$ for a range of Reynolds numbers when a constant translation distance L/D = 3 was employed. This plot is revealing as it verifies observations discerned from the simulated particle tracking images presented here.

Due to the significant diffusion in the flow at Re = 50, no secondary induced vortex was formed. The region of opposite-sign vorticity associated with the backwash boundary layer remained attached to the surface of the cylinder. In this simulation, the wake vortex convected almost normal to the original direction cylinder motion at a slower pace than in the higher-Reynolds-number simulations. In each of the cases from Re = 100 to 1000 a secondary induced vortex was detected, although for Re = 100 this vortex was only observed for $6 < t\text{-}t_{arrest} < 18$. At lower Reynolds numbers, the secondary vortex was observed to be weaker, and as the vortex pair convected away from the cylinder, they diffused more rapidly than in the higher-Reynolds-number cases. This

meant that the distance travelled by the vortex pair at lower Reynolds numbers was shorter than at the higher Reynolds numbers. A curious phenomenon was observed at higher Reynolds numbers, where the longer trajectories traced by the vortices was seen to curve out and backwards, eventually migrating in the opposite direction to the original direction of travel of the cylinder and the wake. At the highest Reynolds number investigated (Re = 1000), the vortices turned so markedly that they began to migrate back towards the wake centreline.
In every case displayed in the plot in figure 6, symmetry about the wake centreline was preserved. This implies that with sufficiently short cylinder translations, the Hopf transition in the wake is given insufficient time to evolve, even with Reynolds numbers 20 times the critical Reynolds number being computed. However, the final image in figure 3 does imply that given sufficiently long translation times, asymmetry will eventually develop in the wakes.

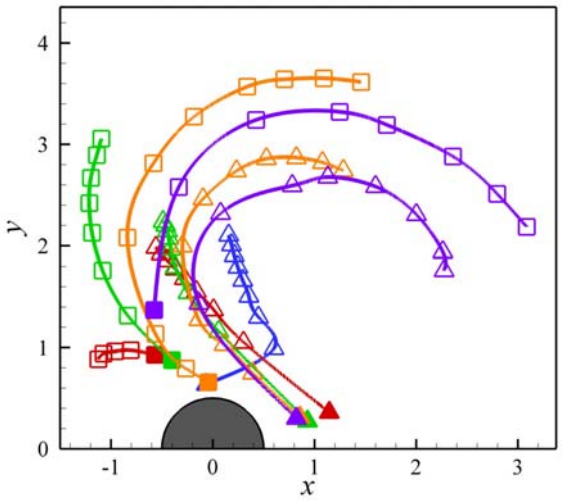

Figure 6: Loci of the cores of the primary wake vortex (Δ) and the secondary induced vortex (□) from time t-t_{arrest} = 0 (solid symbols) through to t-t_{arrest} = 24 (open symbols). A constant L/D = 3 was used, and Reynolds numbers Re = 50 (blue), 100 (red), 200 (green), 500 (orange) and 1000 (purple) are displayed. The circular cylinder is shown in grey. Due to symmetry in the flow, only the trajectories in one half of the wake are shown.

Vortex core trajectories at a constant Reynolds number (Re = 100) are shown in figure 7 for a range of translation distances $1 \leq L/D \leq 10$. This plot demonstrates that at a constant Reynolds number, there is only a weak dependence of the vortex core trajectories on L/D. Notice that especially for the wake vortices, the final path taken was almost independent of translation distance despite the markedly different start locations of each trajectory. The secondary induced vortices tended to be substantially weaker; only emerging at 6 time units after arrest for L/D = 3, 5 and 10, and not being observed at all at lower translation distances.

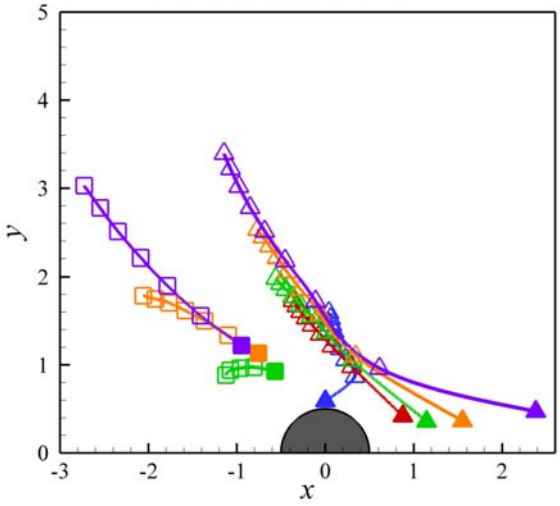

Figure 7: Loci of the cores of the primary wake vortex (Δ) and the secondary induced vortex (□) from time t-t_{arrest} = 0 (solid symbols) through to t-t_{arrest} = 24 (open symbols) for simulations at Re = 100 at L/D = 1 (blue), 2 (red), 3 (green), 5 (orange) and 10 (purple). The circular cylinder is shown in grey. Due to symmetry in the flow, only the trajectories in one half of the wake are shown.

COMPARISON WITH EXPERIMENT

An experimental dye visualization experiment was performed to validate this study. A circular cylinder with a high aspect ratio (greater than 20) was suspended from fine thread in a water tank of generous dimensions (40mm by 40mm wide and 1m high). By coating the cylinder in Fluorescein dye, the wake vortices could be identified by illuminating the dye entraining into the fluid from the cylinder using a blue laser sheet. The comparison in figure 8 demonstrates the excellent degree of similarity in vortex structures and dynamics between the simulations and experiment. This comparison also verifies that in a fashion similar to the delayed onset of the development of the Hopf instability in flows with a short translation distance even at Reynolds numbers far beyond the transition; so too is the transition to three-dimensionality. Here it is seen that over the presented timeframe, at a Reynolds number approximately 2.6 times that of the transition Reynolds number for three-dimensionality in circular cylinder wakes, the experimental visualization compares so closely that it is clear that three-dimensional flow features have either not developed, or are insignificant. This verifies the physicality of the numerical results provided in this study.

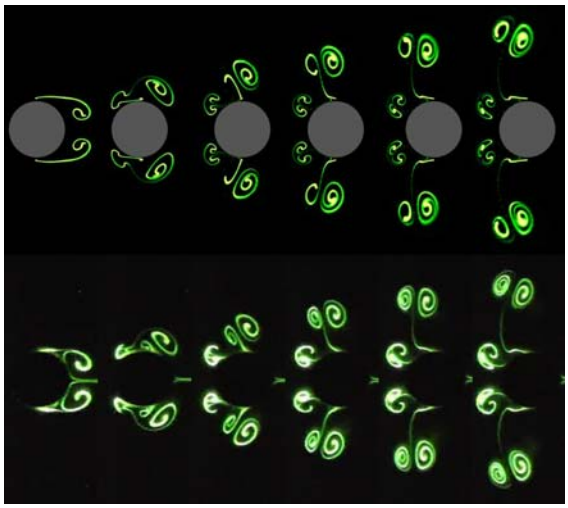

Figure 8: Comparison between the computed particle trace simulations (top) and experimental dye visualization (bottom) for a case with Re = 500 and L/D = 2. From left to right, non-dimensional times t-t_{arrest} = 0, 1, 2, 3, 4, 5 are shown.

A useful direction for future research would be an investigation into the three-dimensional stability of the flows considered here. This would verify the appropriateness of the two-dimensional assumption being imposed on the flows in this study. It was observed experimentally that the computed and observed vortex trajectories deviated after approximately 10 time units, and a numerical stability analysis would assist in determining if this deviation was due to three-dimensional instability in the flow or experimental error.

CONCLUSIONS

A range of translation distances and Reynolds numbers have been investigated for an arresting cylinder. A novel technique for visualization of the computed flows was used whereby simulated particle tracking was used to mimic the entrainment of dye into the wake in experimental dye visualization, and plots of the concentration of particles based on a Gaussian weighted distribution local to each interpolation point permitted comparison with experimental photography.
These simulations have revealed that with a translation distance of three diameters, the vortices around the cylinder tend to deviate sideways and backwards rather than rolling past the cylinder and continuing in its original direction of motion. The viscous effects at lower Reynolds numbers were observed to retard the propagation of the counter-rotating vortex pairs, and at higher Reynolds numbers, the vortices travelled larger distances – in some cases turning back on themselves and meeting again behind the cylinder. For longer translation distances, Hopf instability in the wake eventually destroyed the symmetry about the wake centreline for Reynolds numbers above the transition point.

ACKNOWLEDGEMENTS

The authors wish to thank the Australian Partnership for Advanced Computing (APAC) for providing access to the computing facilities required to complete this study through the merit allocation scheme. G.J.S. received salary through an Australian Postdoctoral Fellowship on ARC Discovery Grant DP0555897. T.L. was supported under the same grant during his stay at Monash University in 2006.

REFERENCES

BARKLEY, D. and HENDERSON, R.D., (1996), "Three-dimensional Floquet stability analysis of the wake of a circular cylinder", *J. Fluid Mech.*, 322, 215-241.

BRAZA, M., CHASSAING, P. and HA MINH, H., (1986), "Numerical study and physical analysis of the pressure and velocity fields in the near wake of a circular cylinder", *J. Fluid Mech.*, 165, 79-130.

COPPOLA, G., SHERWIN, S.J. and PEIRO, J., (2001), "Non-linear particle tracking for high-order elements", *J. Comp. Phys.*, 172, 356-386.

KARNIADAKIS, G.EM., ISRAELI, M. and ORSZAG, S.A., (1991), "High-order splitting methods for incompressible Navier-Stokes equations", *J. Comp. Phys.*, 97, 414-443.

KARNIADAKIS, G.EM. and SHERWIN, S.J., (2005), "Spectral/*hp* element methods for computational fluid dynamics", *Oxford University Press*.

KOUMOUTSAKOS, P. & LEONARD, A., (1995), "High-resolution simulations of the flow around and impulsively started cylinder using vortex method", *J. Fluid Mech.*, 296, 1-38.

LEWEKE, T., THOMPSON, M.C. & HOURIGAN, K., (2004), "Vortex dynamics associated with the collision of a sphere with a wall", *Phys. Fluids*, 16(9), L74-77.

PROVANSAL, M., MATHIS, C. and BOYER, L., "Bénard-von Kármán instability: Transient and forced regimes", *J. Fluid Mech.*, 182, 1-22.

SHEARD, G.J., THOMPSON, M.C. and HOURIGAN, K., (2003), "From spheres to circular cylinders: Stability and flow structures of bluff ring wakes", *J. Fluid Mech.*, 492, 147-180.

THOMPSON, M.C., HOURIGAN, K. and SHERIDAN, J., (1996), "Three-dimensional instabilities in the wake of a circular cylinder", *Exp. Thern. Fluid Sci.*, 12, 190-196.

WILLIAMSON, C.H.K., (1988), "The existence of two stages in the transition to three-dimensionality of a cylinder wake, *Phys. Fluids*, 31(11), 3165-3168.